High-Capacity Dual-Electrolyte Aluminum–Air Battery with Circulating Methanol Anolyte

Pemika Teabnamang [1], Wathanyu Kao-ian [1], Mai Thanh Nguyen [2], Tetsu Yonezawa [2,3], Rongrong Cheacharoen [4] and Soorathep Kheawhom [1,5,*]

[1] Department of Chemical Engineering, Faculty of Engineering, Chulalongkorn University, Bangkok 10330, Thailand; 5970448221@student.chula.ac.th (P.T.); wathanyu.k@student.chula.ac.th (W.K.-i.)

[2] Division of Materials Science and Engineering, Faculty of Engineering, Hokkaido University, Hokkaido 060-8628, Japan; mai_nt@eng.hokudai.ac.jp (M.T.N.); tetsu@eng.hokudai.ac.jp (T.Y.)

[3] Institute of Business-Regional Collaborations, Hokkaido University, Hokkaido 001-0021, Japan

[4] Metallurgy and Materials Science Research Institute, Chulalongkorn University, Bangkok 10330, Thailand; rongrong.c@chula.ac.th

[5] Research Unit of Advanced Materials for Energy Storage, Chulalongkorn University, Bangkok 10330, Thailand

* Correspondence: soorathep.k@chula.ac.th; Tel.: +66-81-490-5280

Abstract: Aluminum–air batteries (AABs) have recently received extensive attention because of their high energy density and low cost. Nevertheless, a critical issue limiting their practical application is corrosion of aluminum (Al) anode in an alkaline aqueous electrolyte, which results from hydrogen evolution reaction (HER). To effectively solve the corrosion issue, dissolution of Al anode should be carried out in a nonaqueous electrolyte. However, the main cathodic reaction, known as oxygen reduction reaction (ORR), is sluggish in such a nonaqueous electrolyte. A dual-electrolyte configuration with an anion exchange membrane separator allows AABs to implement a nonaqueous anolyte along with an aqueous catholyte. Thus, this work addresses the issue of anode corrosion in an alkaline Al–air flow battery via a dual-electrolyte system. The battery configuration consisted of an Al anode | anolyte | anion exchange membrane | catholyte | air cathode. The anolytes were methanol solutions containing 3 M potassium hydroxide (KOH) with different ratios of water. An aqueous polymer gel electrolyte was used as the catholyte. The corrosion of Al in the anolytes was duly investigated. The increase of water content in the anolyte reduced overpotential and exhibited faster anodic dissolution kinetics. This led to higher HER, along with a greater corrosion rate. The performance of the battery was also examined. At a discharge current density of 10 mA·cm^{-2}, the battery using the anolyte without water exhibited the highest specific capacity of 2328 mAh/g$_{Al}$, producing 78% utilization of Al. At a higher content of water, a higher discharge voltage was attained. However, due to greater HER, the specific capacity of the battery decreased. Besides, the circulation rate of the anolyte affected the performance of the battery. For instance, at a higher circulation rate, a higher discharge voltage was attained. Overall, the dual-electrolyte system proved to be an effective approach for suppressing anodic corrosion in an alkaline Al–air flow battery and enhancing discharge capacity.

Keywords: aluminum; aluminum–air battery; flow battery; dual electrolyte; anion exchange membrane; methanol; potassium hydroxide

1. Introduction

Aluminum–air batteries (AABs) offer an attractive combination of low cost, lightweight, and ultrahigh energy density [1,2]. AABs exhibit a high specific capacity of 2.98 Ah/g$_{Al}$, which is

the second highest after that of Li–air batteries (LABs; 3.86 Ah/g_{Li}) and much higher than zinc–air batteries (ZABs; 0.82 Ah/g_{Zn}) [3–5]. AABs also provide other benefits, such as low environmental impact and high safety. Nonetheless, AABs have long experienced significant difficulty arising from corrosion of aluminum (Al) anode, which results from the parasitic hydrogen evolution reaction (HER). The corrosion causes additional consumption of the Al anode, leading to unacceptably low utilization efficiency [6]. Besides, it leads to the production and accumulation of hydrogen gas in the cell. Consequently, this increases the possibility of hydrogen explosion. These issues have prevented widespread usage of AABs.

Approaches to mitigate corrosion of the Al anode have been proposed, such as (1) alloying Al with other metals [7–9], (2) coating the Al anode with ceramics [10,11], (3) introducing additives to the electrolyte [12,13], (4) applying gel electrolytes [14], (5) using nonaqueous electrolytes, [15] and (6) operating at low temperature [16]. However, these efforts have revealed minimal success and have often increased the intricacy of the battery system.

To effectively address the corrosion issue, Al oxidation should be carried out in a nonaqueous electrolyte. However, in such a nonaqueous electrolyte, oxygen reduction reaction (ORR), which is the most important cathodic reaction, is inadmissibly sluggish. An aqueous electrolyte is usually required to favor ORR. Thus, a dual-electrolyte AAB using an anion exchange membrane to separate the anolyte and the catholyte was developed [17]. This setup offered flexibility in implementing the very different anolyte and catholyte. By applying a suitable anolyte, HER at the anode could be significantly suppressed, and a high-performance battery could be attained.

Al dissolution in an alkaline aqueous solution involves repetitive generation and breaking down of the thin Al_2O_3 layers over the Al surface [18]. The anodic dissolution of Al is controlled via the through-film dissolution process. Alternative anolyte solutions have been explored, such as ethylene glycol and methanol. In the ethylene glycol solution, it was reported that the precipitation of aluminum hydroxide was the main phenomenon affecting the Al corrosion [19]. An amount of 4 M sodium hydroxide in ethylene glycol containing different dicarboxylic acid compounds was examined in AABs using AA5052 Al anode [20]. In alkaline ethylene glycol solution, dicarboxylic acid additives enhanced electrochemical activity and discharge performance of AA5052 Al alloy. Methanol was seen to provide excellent corrosion inhibition in alkaline solution electrolyte [21,22]. Methanol was employed in dual-electrolyte AABs and led to very high discharge capacity. In this system, methanol was implemented as the anolyte, and an aqueous electrolyte was employed as the catholyte [17]. However, its performance was still limited by passivation of oxide products accumulated on the Al surface.

Passivation of the anode, which results from the accumulation of discharged products on the surface of the anode, is another critical issue. It has been reported that the passivation problem can be effectively solved by introducing a flowing electrolyte. By circulating electrolyte continuously to minimize the concentration gradient of the discharge product, it was noticed that anode passivation could be suppressed [5,23,24]. Though flow battery structure offers significant benefits, it has not been implemented in a dual-electrolyte configuration.

In this work, the issue of Al corrosion in an Al–air flow battery (AAFB) was resolved by implementing a dual-electrolyte configuration. Electrochemical behavior of the Al anode was duly examined in methanol solutions containing 3 M potassium hydroxide (KOH) with different ratios of water. Hydrogen evolution (gasometry) measurements, Tafel polarization, electrochemical impedance spectroscopy (EIS), and scanning electron microscopy (SEM) were carried out. Further, a dual-electrolyte AAFB was implemented using a structure of an Al anode| methanol solution anolyte | anion exchange membrane | polymer gel catholyte | air cathode along with a circulation anolyte. Subsequently, the performance of the battery under the effects of water content in the electrolyte and circulation rate of the anolyte was examined.

2. Materials and Methods

2.1. Materials

Aluminum plates (99.99%, Qijing Trading Co., Ltd., Fuzhou, China) were used as working electrodes in the half-cell test and anodes in AAFB. Nickel foam (99.97%, 100 PPI, 1 mm thick, Qijing Trading Co., Ltd., Fuzhou, China) was used as the cathode current collector. The electrolyte of the half-cell test and the anolyte of the battery was prepared from methanol (99.8%) and potassium hydroxide pellets (KOH, 99%), purchased from QRëC, Auckland, New Zealand. The cathode was prepared using carbon black (Vulcan$^®$ BP2000, Cabot Corporation, Boston, MA, USA), polytetrafluoroethylene (PTFE powder, 1 μm, Sigma-Aldrich, St. Louis, MO, USA), toluene (99.5%, Loba Chemie Pvt. Ltd., Mumbaia, India), ethanol (99.8%, QRëC, Auckland, New Zealand), poly(styrene-co- butadiene) (Sigma-Aldrich, St. Louis, MO, USA), and manganese (IV) oxide (MnO_2, 5 μm, 99.99%, Sigma-Aldrich, St. Louis, MO, USA). Carbopol$^®$ 940 polymer (CBP940), supplied by Lubrizol Corporation, Wickliffe, OH, USA, was used to prepare the catholyte. All chemicals were used as accepted, without any further purification. In the battery, the anolyte and the catholyte were separated by an anion-exchange membrane (AMI-7001S, Membrane International Inc., Ringwood, NJ, USA).

2.2. Hydrogen Evolution and Half-Cell Test

Figure 1a demonstrates the setup employed for the measurement of HER. Hydrogen evolution tests were carried out during 60 min of immersion in methanol solutions containing 3 M KOH with different ratios of water (0%, 5%, 10%, and 20% (v/v)) at 30 °C. Before the test, Al samples were cleaned five times using methanol. Thus, an Al sample, 1.5 cm^2 in area, was put into a beaker containing 50 mL of the solution. Next, a funnel was positioned over the sample, ensuring the accumulation of all the hydrogen from the sample. Next, a burette was installed over the funnel and was initially full of the electrolyte. The hydrogen that was in the funnel passed into the burette and gradually displaced the electrolyte. The burette allowed the volume of evolved hydrogen gas to be measured as a function of time. Reaction rates were determined by the slope of the straight lines in the gasometry plots.

A half-cell test was carried out to examine corrosion of the Al anode in methanol solutions containing 3 M KOH with different ratios of water (0%, 5%, 10%, and 20% (v/v)). A three-electrode configuration was used to study electrochemical characterization. The three-electrode cell consisted of a platinum (Pt) counter electrode of 10×10 mm^2, a Ag/AgCl reference electrode, and an Al plate working electrode of 10×10 mm^2. The aluminum working electrode was rinsed three times with acetone before being tested at room temperature. A potentiostat/galvanostat (PAR VersaSTAT 3A, Ametek Inc., Berwyn, PA, USA) was employed to study EIS and Tafel polarization. EIS was examined at a frequency range of 200 kHz to 0.2 Hz and voltage excitation of 5 mV at open-circuit voltage (OCV). EIS was carried out to examine the corrosion of Al samples immediately after immersion in the solutions and after being immersed in the solutions for 90 min. Besides, Tafel polarization was performed at a scan rate of 5 mV·s^{-1} in the potential region cover at −500 mV vs. OCV to 0 V vs. Ag/AgCl. EIS using a frequency range of 1 Hz to 100 kHz with the excitation voltage of 10 mV$_{RMS}$ was also applied to measure ionic conductivity of the methanol solutions. The cell setup was composed of two chambers with a 10×10 mm^2 stainless steel (SUS316) electrode. The bulk resistance, determined from an equivalent circuit model, was then used to calculate the ionic conductivity of the solutions [25].

Further, morphology of the Al surface before and after being immersed in methanol solutions for 45 min was studied via SEM using a field emission SEM (ZEISS Sigma 500, Carl Zeiss AG, Oberkochen, Germany) at an accelerating voltage of 5 kV at a working distance between 1 and 5 mm. SEM was carried out on Al samples before and after being immersed in the solutions for 45 min.
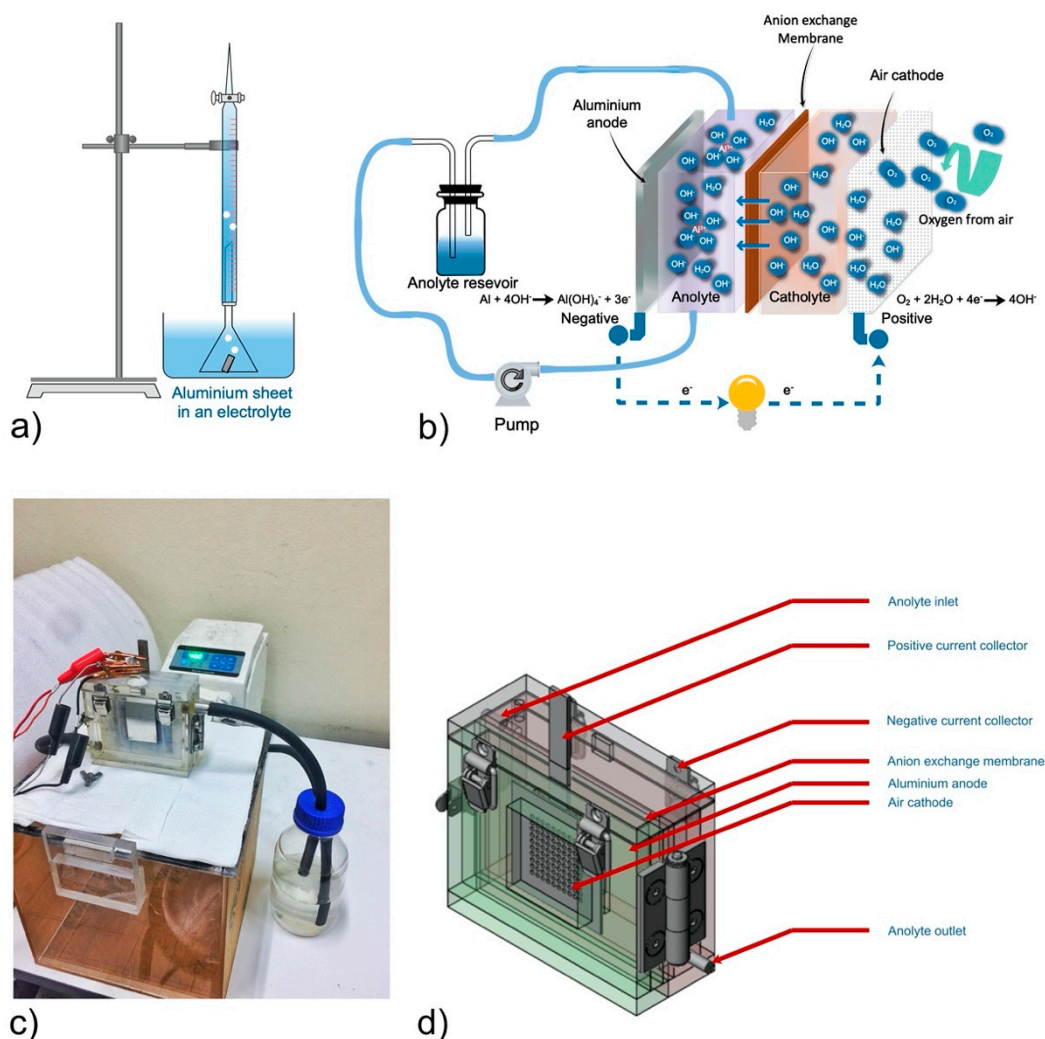
Figure 1. (**a**) Experimental setup for hydrogen evolution measurement. (**b**) Schematic diagram of a dual–electrolyte Al–air battery (AAB) with circulating anolyte. (**c**) Photographic image of the battery setup. (**d**) Design of the dual-electrolyte Al–air battery cell

2.3. Full-Cell Test

Figure 1b shows a schematic illustration of the dual-electrolyte Al–air battery with flowing anolyte. The anode electrode was $30 \times 50 \times 0.19$ mm^3 and weighed 0.8 g. The methanol solutions containing 3 M KOH with different ratios of water (0%, 5%, 10%, and 20% (v/v)) were used as the anolyte. The catholyte was a polymer gel electrolyte consisting of 3 M KOH dissolved in deionized water. Then, CBP940 (1.2 wt %) was added to each condition. The gel electrolyte offered satisfactory mechanical properties and reduced electrolyte loss due to evaporation. An anion-exchange membrane of 30×30 mm^2 was used to separate the anolyte and the catholyte. The anion-exchange membrane was activated by soaking in 5 M NaCl aqueous solution for 24 h at 30 °C. The cathode electrode consisted of three layers: a catalyst layer, a cathode current collector, and a gas diffusion layer. The cathode current collector was nickel (Ni) foam. The catalyst layer was in contact with the catholyte. The active area of the cathode reaction was 4 cm^2. The catalyst layer was fabricated by casting a slurry mixture of MnO$_2$ (0.3 g) as the ORR catalyst, with carbon BP2000 (0.7 g) and poly(styrene-co-butadiene) (0.1 g) dispersed in 10 mL of toluene. The coated Ni foam was pressed at 150 °C for 10 min using a manual hot press. To fabricate the gas diffusion layer, the outer surface of the air cathode was prepared by coating a mixture of carbon XC-72 and PTFE binder in 10 mL ethanol with a ratio of 80:20 wt/wt, respectively. The well-dispersed paste was applied onto the other side of the nickel foam and then pressed using a

manual hot press at 350 °C for 15 min. The gas diffusion layer exhibited hydrophobicity and prevented leaking of the electrolyte whilst enabling oxygen gas to diffuse to the cell. The operation of the battery was carried out at 15 °C to minimize evaporation of the methanol solutions.

In Figure 1c, a photographic image of the battery used in the experiment is shown. Figure 1d displays the cell design, which consisted of an aluminum anode, a chamber for the anolyte, an anion exchange membrane (acting as a separator), a chamber for the catholyte, as well as the air cathode. The distance between the cathode and anode electrodes was 18 mm. Further, both the battery discharge capacity and voltage–current polarization characteristic were analyzed by a battery testing system (CT-4008-5V20mA, Neware Technology Ltd., Shenzhen, China).
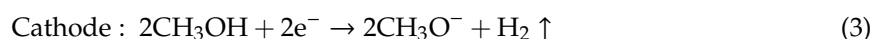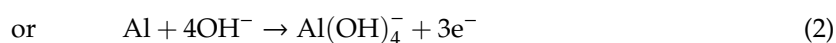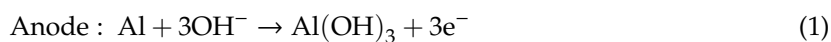
3. Results and Discussion

Figure 2a shows the relationship between hydrogen gas evolution as a function of time. The linear variation for the volume of hydrogen gas evolved in time varied with water content in the methanol solutions. The volume of hydrogen represents how much aluminum in AABs was consumed by HER without electricity generation.
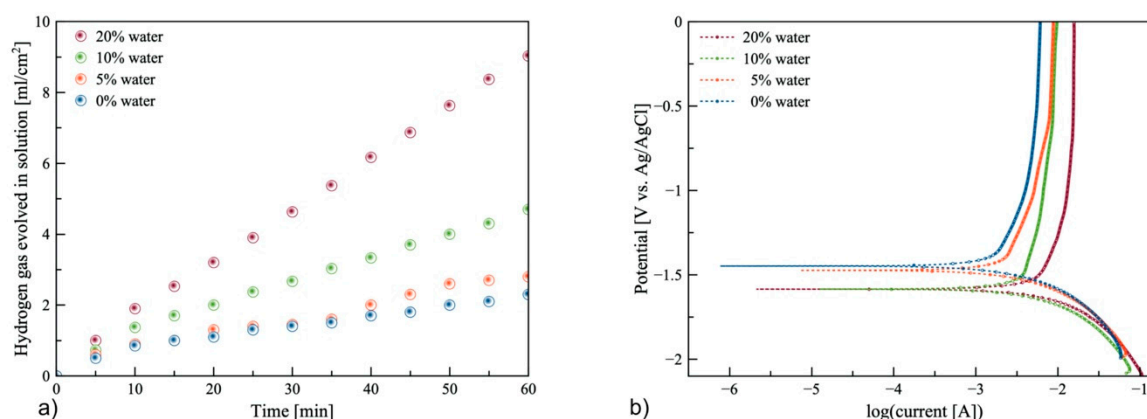
Figure 2. (**a**) Hydrogen gas evolved from an Al sample in methanol solutions containing 3M potassium hydroxide (KOH) with different ratios of water (0%, 5%, 10%, and 20% (v/v)). (**b**) Tafel polarization of an Al electrode in methanol solutions containing 3 M KOH with different ratios of water (0%, 5%, 10%, and 20% (v/v)).

The condition of 0% water exhibited the hydrogen evolution rate of 0.017 mL·cm^{-2}min^{-1}, while the condition of 5%, 10%, and 20% water showed hydrogen rates of 0.021, 0.036, and 0.074 mL·cm^{-2} min^{-1}, respectively. The corrosion of Al could also take place in the case of 0% water (anhydrous) KOH methanol solution, thereby producing hydrogen gas. The corresponding reactions are shown in Equations (1)–(3) [21]:

$$\text{Anode}: \ \text{Al} + 3\text{OH}^- \rightarrow \text{Al(OH)}_3 + 3\text{e}^- \tag{1}$$

$$\text{or} \quad\quad \text{Al} + 4\text{OH}^- \rightarrow \text{Al(OH)}_4^- + 3\text{e}^- \tag{2}$$

$$\text{Cathode}: \ 2\text{CH}_3\text{OH} + 2\text{e}^- \rightarrow 2\text{CH}_3\text{O}^- + \text{H}_2 \uparrow \tag{3}$$

Accordingly, two anodic reactions, which were related to the dissolution of Al, were involved. The cathodic reaction involved the reduction of methanol and produced hydrogen gas. However, as shown in Equation (4), when the electrolyte contained water, reduction of water could also occur, leading to hydrogen gas production. In both cases, hydrogen gas production was possible. However, the hydrogen production rate regarding the 3 M KOH anhydrous electrolyte was much slower than that of the electrolyte containing water, as shown in Equation (4):

$$\text{Cathode}: \ 2\text{H}_2\text{O} + 2\text{e}^- \rightarrow 2\text{OH}^- + \text{H}_2 \uparrow \tag{4}$$
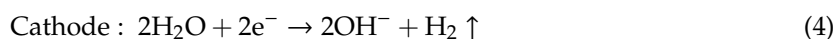
Figure 2a also indicates that HER was higher when the water content increased. The diagram further shows that the highest amount of hydrogen gas evolved was observed in the condition of 20% water, which was the highest water content studied in this work.

Tafel polarization was investigated via a three-electrode cell, namely, an Al working electrode, a Ag/AgCl reference electrode, and a platinum counter electrode. Figure 2b shows the Tafel polarization of Al in 3 M KOH methanol solutions with different ratios of water (0%, 5%, 10%, and 20% (v/v)). The OCV of the 3 M KOH anhydrous methanol electrolyte (0% water) was detected at −1.45 V. The OCV of the electrolytes containing water showed a negative shift as water content increased. The negative shift of OCV indicated a higher tendency of hydrogen evolution or corrosion of Al. The polarization resistance and other related properties were calculated using Butler–Volmer and Stern–Geary equations [26,27], as shown in Equations (5) and (6):

$$I = I_{\text{corr}} \left(e^{\frac{2.303(E - E_{\text{corr}})}{\beta_a}} - e^{\frac{2.303(E - E_{\text{corr}})}{\beta_c}} \right) \tag{5}$$

$$R_p = \frac{\beta_a |\beta_c|}{2.303 I_{\text{corr}} (\beta_a + |\beta_c|)} \tag{6}$$

where, I is the measured current density, I_{corr} is the corrosion current density, E is the electrode potential, E_{corr} is the corrosion potential, and β_a and β_c are the anodic and cathodic Tafel slopes, respectively. By approximating the Tafel slopes as a straight line, the polarization resistance (R_p) can be estimated. R_p is the transition resistance between the electrode and the electrolyte. Table 1 displays Tafel polarization parameters consisting of corrosion potential (E_{corr}), corrosion current density (I_{corr}), anodic slope (β_a), cathodic slope (β_c) and polarization resistance (R_p).

Table 1. Results of Tafel polarization of Al in 3 M KOH in methanol solutions containing different ratios of water (0%, 5%, 10%, and 20% (v/v)).

% Water	E_{corr} (V vs. Ag/AgCl)	I_{corr} (A·cm^{-2})	β_a (V·dec^{-1})	β_c (V·dec^{-1})	R_p (Ω)
0% water	−1.4	0.002	1.05	−6.18	252.31
5% water	−1.5	0.003	0.86	−5.50	119.04
10% water	−1.5	0.004	0.71	−4.88	61.11
20% water	−1.5	0.006	0.63	−3.60	36.71

Corrosion rate is proportionally related to polarization resistance; higher polarization resistance indicates lower corrosion current. Therefore, higher polarization resistance indicates greater corrosion inhibition property. The anodic slope shows the corrosion tendency of the anode, in other words, how a large overpotential is required to drive the reaction [28].

Results showed that polarization resistance decreased as the amount of water in the electrolyte increased. The smallest slope (0.63 V·dec^{-1}) and smallest polarization resistance (36.71 Ω) provided by the electrolyte containing 20% water indicated the highest corrosion tendency of Al. The corrosion current density of the solution with 20% water was 0.006 A·cm^{-2}. In comparison, the highest anodic Tafel slope (1.05 V·dec^{-1}) occurred in the 3 M KOH anhydrous methanol electrolyte. Thus, the corrosion current density of the 3 M KOH anhydrous methanol electrolyte was found to be 0.002 A·cm^{-2}, while the polarization resistance was 252.31 Ω. Though the higher polarization proved to have a decisive advantage in the corrosion inhibition of Al, it had negative effects on battery performance as higher overpotential is required for Al dissolution.

EIS technique was applied to study the characteristic of the Al dissolution process as well as the behavior of Al corrosion. Figure 3 displays Nyquist plots of Al in 3 M KOH methanol solutions containing different ratios of water (0%, 5%, 10%, and 20% (v/v)). All plots showed a similar characteristic. Similar plots were also reported for Al in alkaline aqueous solution [29]. The impedance

spectra consisted of a large capacitive loop at high frequency, a small inductive loop at middle frequency, and a second small capacitive loop at low frequency. The capacitive semicircle at high frequency was ascribed to the redox reaction of $Al \leftrightarrow Al^+$. This loop was found to be the rate-determining step in the charge transfer process [30]. The inductive loop at middle frequency resulted from an adsorption of intermediates on the Al surface. The adsorption of intermediate species, such as $Al(OH)_3$ and $Al(OH)_4{}^-$, were involved in the Al dissolution process. The other capacitive semicircle at low frequency was attributed to the $Al^+ \leftrightarrow Al^{3+}$ redox reaction [31]. It is significant that Al dissolution in the alkaline aqueous solution involves the dissolution of Al_2O_3 film over the Al surface, leading to repeated Al_2O_3 film dissolution and formation of a relatively thin Al_2O_3 film [18]. Subsequently, Al^{3+} ions, oxidized at the Al_2O_3 film interface, migrate across the film to the bulk electrolyte. Simultaneously, the migration of O^{2-} ions, generated at the film/electrolyte interface, are responsible for continued generation of Al_2O_3 at the film interface. Thus, the anodic dissolution of Al is controlled by the through-film dissolution of Al. In other words, such redox reactions occur according to the aluminum hydrous layer formation and subsequent precipitation of $Al(OH)_3$.
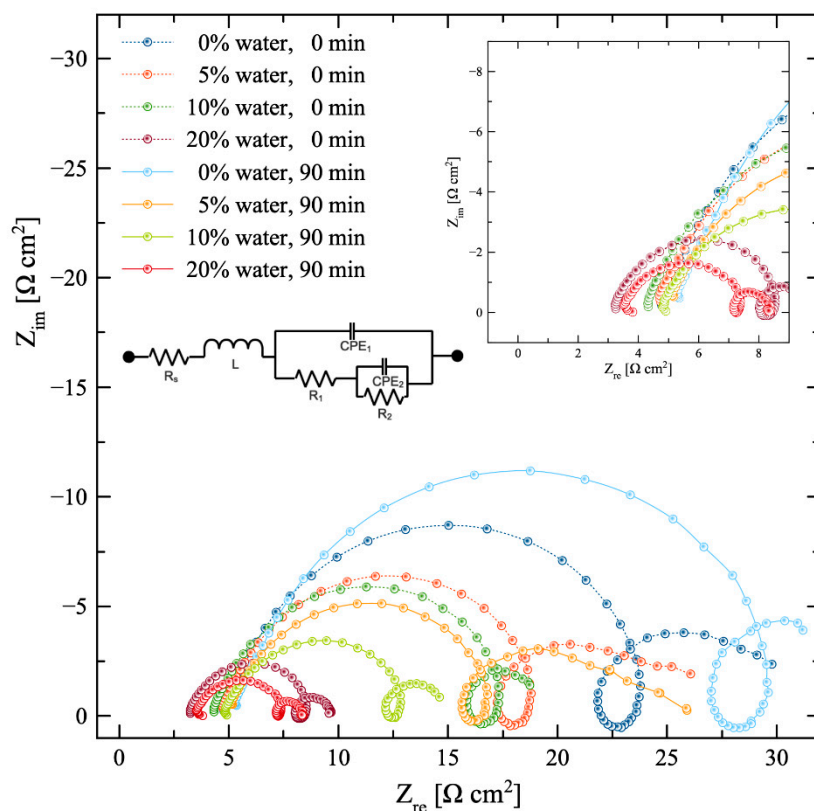
Figure 3. Nyquist plots of electrochemical impedance spectroscopy (EIS) of an Al electrode in methanol solutions containing 3 M KOH with different ratios of water (0%, 5%, 10%, and 20% (v/v)).

In the case of KOH methanol electrolytes, it is possible that methyl oxide (CH_3O^-) may inhibit the reaction of OH^- and Al^{3+}, which are the main reactants producing $Al(OH)_3$ and $Al(OH)_4{}^-$. Besides, CH_3O^- forms a more stable oxide film over the Al surface. However, the migration of Al^{3+} through the film in this case was found to be slower than that of the aqueous alkaline solution. The 3 M KOH anhydrous electrolyte displayed the highest diameter of capacitive and inductive loops. However, when water content increased, it led to a decrease in the diameter size of the capacitive loop because a higher amount of OH^- was produced. Moreover, an increase in water content can reduce charge transfer resistance. Consequently, the corrosion rate increased. In addition, the solution resistance negatively shifted.

Furthermore, in Figure 3, the Nyquist plots of Al anode in 3 M KOH methanol solutions at immediate immersion of Al and after 90 min are shown. It was found that, regarding the 3 M KOH anhydrous methanol electrolyte, only the diameter of the capacitive and inductive loops increased after 90 min immersion. This was due to the slow reaction of Al–CH$_3$O$^-$. The resulting film showed a higher corrosion inhibition effect than the pristine Al surface. The film produced by the reaction of Al–CH$_3$O$^-$ could effectively suppress Al corrosion. Besides, when water was introduced to the electrolyte, the width of the capacitive semicircle decreased with time due to the Al corrosion caused by the Al dissolution process. The film produced in the presence of water exhibited a lower corrosion inhibition effect than the pristine Al surface. Results thus indicated that the presence of water in the solution led to higher corrosion tendency of Al.

Table 2 shows the EIS parameters for Al in 3 M KOH in methanol solutions with different ratios of water content as determined via fitting with an equivalent circuit model. The model included the effects of solution resistance (R_s), constant phase elements (CPE_1 and CPE_2), and charge transfer resistances (R_1 and R_2). Charge transfer resistances are the result of the kinetically controlled electrochemical reaction, while the constant phase elements represent the double layer capacitance, which arises from the absorption of charged species, at the electrode/electrolyte interface. Results indicated that the solution resistance of the Al dissolution process significantly decreased as water content increased. Moreover, as water content increased, there was a decrease in the double layer capacitance as well as in the charge transfer resistance at the electrode/electrolyte interface. Results thus confirmed that water helped decrease the double layer of Al in the dissolution process. In addition, the water content affected ionic conductivity of the solution. The ionic conductivity increased substantially as the water content increased. It was therefore further confirmed that water improved the Al dissolution process.

Table 2. Results of EIS studies of Al in 3 M KOH methanol solutions containing different ratios of water (0%, 5%, 10%, and 20% (v/v)) and ionic conductivity of the methanol solutions.

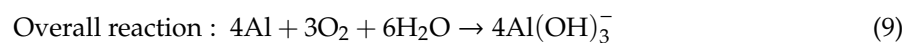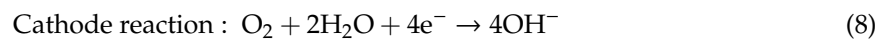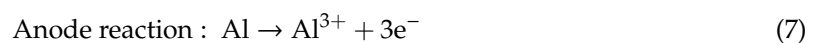| % Water	R_s ($\Omega \cdot cm^2$)	CPE_1 (S·cm^2 s^{-n})	R_1 ($\Omega \cdot cm^2$)	R_2 ($\Omega \cdot cm^2$)	CPE_2 (S·cm^2 s^{-n})	Ionic Conductivity (mS.cm^{-1})
0% water	2.23	19.38	39.76	13.05	6.82	29.24
5% water	1.46	12.19	34.23	16.72	18.94	38.08
10% water	1.23	10.16	23.26	6.68	7.18	46.19
20% water	0.38	3.40	8.82	9.94	4.15	64.87

Figure 4 shows SEM images of Al samples before and after being immersed in 3 M KOH solutions (aqueous solution (Figure 4b), anhydrous methanol solution (Figure 4c), and methanol solution with 5% (v/v) water (Figure 4d)) for 45 min. The SEM image of pristine Al (Figure 4a) depicted a fairly smooth surface, while SEM images of Al samples after immersion in the KOH solutions (Figure 4b–d) exhibited a rough surface with the presence of a number of voids resulting from anodic oxidation of Al. In 3 M KOH aqueous solution, the Al surface contained a large number of very small corrosion pits. These corrosion pits were formed via anodic corrosion initiated by HER. The oxide film that resulted from the corrosion process was loose and porous. In 3 M KOH anhydrous methanol solution, broad shallow corrosion pits with a more compact surface were observed. In the methanol solution containing 3 M KOH with 5% (v/v) water, the Al surface was similar to what was observed in 3 M KOH aqueous solution. The results suggested that the existence of water in the solution led to a loose and porous oxide film on the Al surface. The porous surface structure accelerated the transfer of the reactive species between the Al surface and the electrolyte; thus, the electrolyte containing water showed higher corrosion tendency of Al.
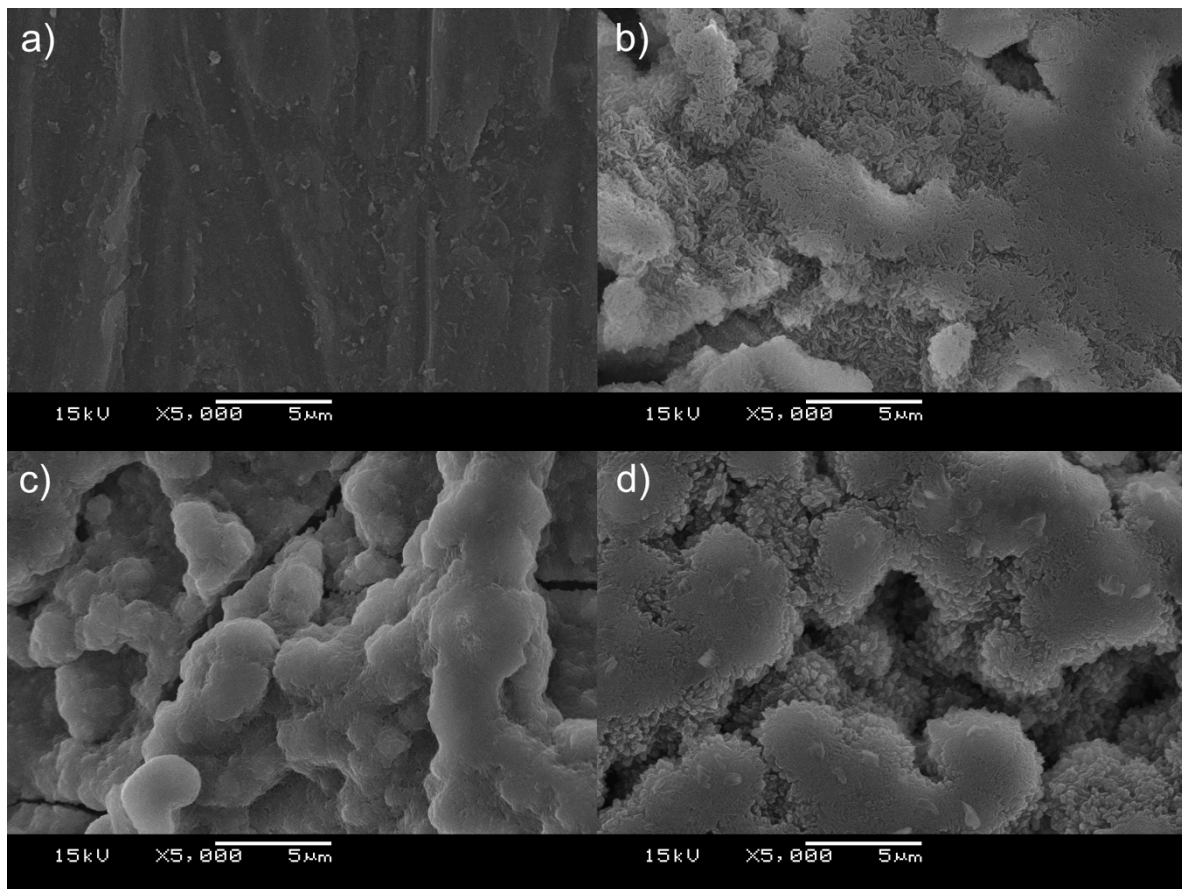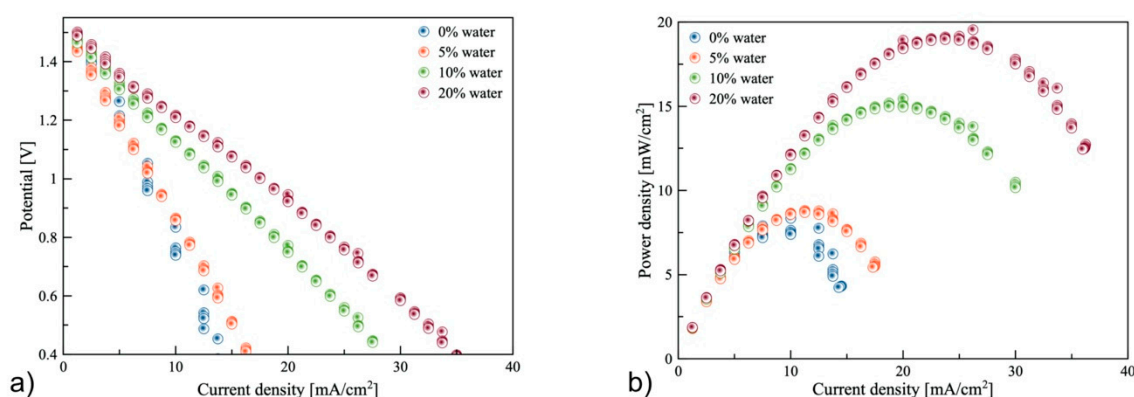
Figure 4. SEM images of Al samples: (**a**) pristine Al, (**b**) after immersion in 3 M KOH aqueous solution for 45 min, (**c**) after immersion in 3 M KOH methanol solution (anhydrous) for 45 min, and (**d**) after immersion in methanol solution containing 3 M KOH with 5% (v/v) water for 45 min.

Following the examination of Al dissolution, the performance of the dual-electrolyte Al–air flow battery was investigated. The effects of methanol-based anolytes containing different ratios of water content were studied. Figure 5 presents the polarization characteristics of the battery. The electrochemical reactions involved in a traditional single aqueous alkaline electrolyte are shown in Equations (7)–(9) [2]:

$$\text{Anode reaction}: \text{Al} \rightarrow \text{Al}^{3+} + 3\text{e}^- \tag{7}$$

$$\text{Cathode reaction}: \text{O}_2 + 2\text{H}_2\text{O} + 4\text{e}^- \rightarrow 4\text{OH}^- \tag{8}$$

$$\text{Overall reaction}: 4\text{Al} + 3\text{O}_2 + 6\text{H}_2\text{O} \rightarrow 4\text{Al(OH)}_3^- \tag{9}$$

Figure 5. (**a**) Polarization characteristics of the dual-electrolyte Al–air battery using an anolyte of methanol solutions containing 3 M KOH with different ratios of water (0%, 5%, 10%, and 20% (v/v)). (**b**) Power density as a function of current density for the dual-electrolyte Al–air battery using an anolyte of methanol solutions containing 3 M KOH with different ratios of water (0%, 5%, 10%, and 20% (v/v)).

Besides, Al also suffers a severe parasitic reaction, as shown in Equation (10):

$$\text{Parasitic reaction}:\ 2Al + 6H_2O + 2OH^- \rightarrow 2Al(OH)_4^- + 3H_2 \uparrow \tag{10}$$
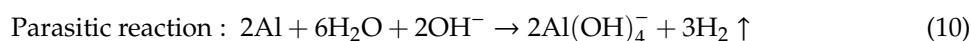
It was observed that the limiting current density of the battery (at the discharge voltage of 0.3 V) for each condition increased slightly, as follows: 15, 18, 30, and 36 mA·cm^{-2} at 0%, 5%, 10%, and 20% water, respectively. Maximum power density was calculated via current density and voltage, providing 7.5, 8.5, 15.4, and 19.6 mW·cm^{-2}, respectively. The battery exhibited linear polarization characteristics. The OCV of 3 M KOH anhydrous methanol electrolyte was 1.44 V. When the deionized water increased to 5%, 10%, and 20%, the OCVs were 1.45, 1.47, and 1.50 V, respectively. It was evident that by increasing the water content, OCV improved. However, it produced a significantly higher hydrogen evolution rate. Table 3 summarizes the maximum current density, power density, and internal resistance of the battery.

Table 3. The maximum current density, power density, and internal resistance of the dual-electrolyte AAB using an anolyte of methanol solutions containing 3 M KOH with different ratios of water (0%, 5%, 10%, and 20% (v/v)).

% Water	Maximum Current Density (mA·cm^{-2})	Maximum Power Density (mW·cm^{-2})	Internal Resistance (Ω)
0%	15	7.5	76.70
5%	18	8.5	65.70
10%	30	15.4	39.24
20%	36	19.6	33.09

The internal resistances observed in each case were 76.70, 65.70, 39.24, and 33.09 Ω at 0%, 5%, 10%, and 20% (v/v) water, respectively. Internal resistance decreased as water content increased; the results were in line with the EIS results. The presence of water in the electrolyte enhanced ionic conductivity. The presence of water also improved the performance of the battery because of its higher activity and ionic conductivity and thereby promoted Al dissolution.

Figure 6 presents discharge profiles of the battery using 3 M KOH in methanol solution anolytes containing different ratios of water (0%, 5%, 10%, and 20% (v/v)). One hour before the test, the anion membrane was put in the cell, and the electrolyte was circulated without an Al anode. The discharge profiles of the battery discharged at a current density of 10 mA·cm^{-2} are presented. Table 4 summarizes the specific capacity, utilization percentage, and discharge time for each condition.
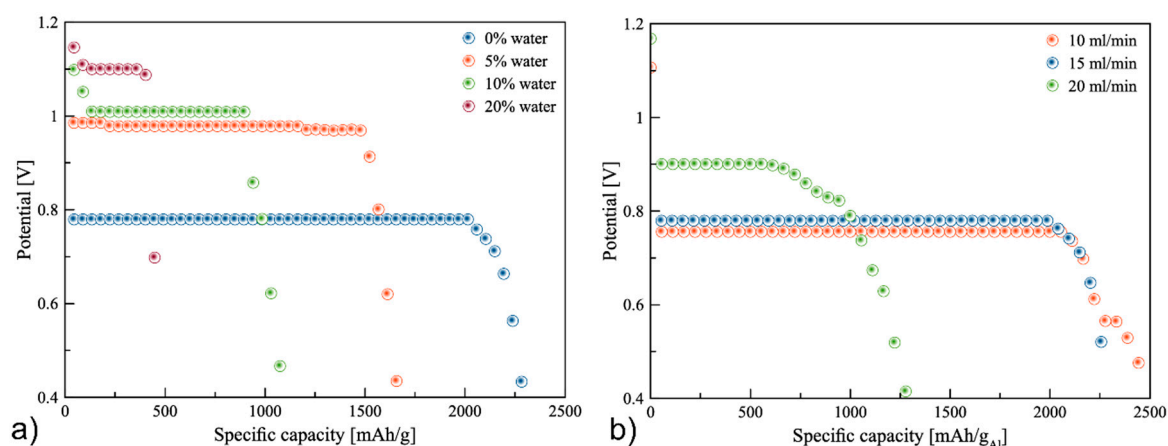
Figure 6. (**a**) Galvanostatic discharge profiles of the batteries using 3 M KOH in methanol solution anolytes containing different ratios of water (0%, 5%, 10%, and 20% (v/v)) and a circulation rate of anolyte of 15 mL/min at discharge current density of 10 mA·cm^{-2}. (**b**) Galvanostatic discharge profiles of the batteries using 3 M KOH anhydrous methanol anolyte with different electrolyte circulation rates at discharge current density of 10 mA·cm^{-2}.

Table 4. Summary of the specific capacity, utilization percentage, and discharge time of the batteries using 3 M KOH in methanol solution anolytes containing different ratios of water (0%, 5%, 10%, and 20% (v/v)) and a circulation rate of anolyte of 15 mL/min at discharge current density of 10 mA·cm^{-2}.

% Water	Discharge Voltage (V)	Specific Capacity (mAh/g$_{Al}$)	Utilization Percentage	Discharge Time (hours)
0%	0.77	2328	78%	~40
5%	0.98	1700	57%	~28
10%	1.02	1130	38%	~18
20%	1.10	465	16%	~7

It can be seen that, in the 3 M KOH anhydrous anolyte, the battery reached the highest specific capacity of 2328 mAh/g$_{Al}$, achieving utilization efficiency of 78%. Moreover, the battery could discharge at 0.87 V continuously for 40 h. Thus, this proved that the Al–air flow battery could exhibit a significantly higher coulombic efficiency using the 3 M KOH anhydrous methanol electrolyte. Accordingly, the hydrogen evolution rate was around 0.017 mL·cm^{-2} min^{-1}, which was the lowest, emphasizing the fact that the parasitic reaction was significantly suppressed. However, when water content increased, specific capacity decreased successively, i.e., 1700, 1130, and 465 mAh/g$_{Al}$ at the condition of 5%, 10%, and 20% (v/v) water, respectively. Simultaneously, when water content increased, the average discharge voltage was enhanced, but the utilization percentage decreased. It is noted that the condition of 5% water could boost discharge voltage and provide utilization percentage of around 57% at a discharge voltage of 0.98 V for 28 h.

The battery using the anhydrous methanol anolyte proved to be the most effective in inhibiting anodic corrosion and provided the highest capacity. It was further investigated by employing different circulation rates, i.e., 10, 15, and 20 mL·min^{-1}. Figure 6b shows the discharge profiles at different circulation rates of anolyte at a current density of 10 mA·cm^{-2}. The highest specific capacity occurred at 10 mL·min^{-1}, while the discharge voltage was 0.75 V. At a circulation rate of 10 mL·min^{-1}, the average discharge voltage was found to be minimal because the circulation rate was minimal. Accordingly, this resulted in the accumulation of discharge products on the Al surface, the accumulation of which produced thick oxide films on the Al surface. Consequently, this led to greater charge transfer resistance and lower discharge voltage. In comparison, at 20 mL·min^{-1}, specific capacity dropped significantly as a high flow rate thinned down the oxide films accumulated on the Al surface and decreased charge

transfer resistance. However, the higher circulation rate brought about lower utilization percentage of Al.

Table 5 shows a comparison of the battery developed in this work and other AABs that have been previously reported. The dual-electrolyte AAFB showed the highest specific capacity. Results may differ depending on different parameters, such as ORR catalyst, electrolyte, and cell configuration. A previous study [17] suggested that Al passivation occurred after discharging for 4–5 h with Al in methanol–KOH solution. It was reported that the discharge time was less than 20 h, which was much lower than the system with anolyte circulation reported herein. This short discharge time was due to the passivation of the Al surface. The dual-electrolyte AAFB developed in this work exhibited lower power density. However, the power density depends on various parameters viz. ORR catalyst, catholyte, and the structure of gas diffusion layer. More advanced ORR catalysts and different catholytes can be applied to enhance the power density. In addition, further studies of other anolytes, such as ethylene glycol and glycerol solutions, implemented in dual-electrolyte AAFB are recommended.

Table 5. Comparison of the battery developed in this work and other AABs that have been previously reported.

System	Air Cathode	Maximum Power Density $(mW \cdot cm^{-2})$	Maximum Specific Capacity (mAh/g_{Al})	References
Dual-electrolyte AAFB (3 M KOH anhydrous methanol anolyte)	MnO_2/C	7.5	2328	This work
Dual-electrolyte AAB (3 M KOH anhydrous methanol anolyte)	Pt/C	28	1810	[17]
Solid state rechargeable AAB	TiN	N/A	35.8	[32]
Paper-based AAB	C	0.8	N/A	[33]
Paper-based solid electrolyte AAB	Ag/C	3.8	900.8	[34]

4. Conclusions

In this work, corrosion of Al in 3 M KOH methanol solutions containing different ratios of water was studied and implemented as a circulating anolyte for a dual-electrolyte AAB. The results of HER revealed excellent corrosion inhibition of 3 M KOH anhydrous methanol solution. However, an increase in corrosion tendency followed the increase in water percentage. Tafel polarization and EIS confirmed that 3 M KOH anhydrous methanol solution exhibited the largest overpotential and highest polarization resistance. It was noted that overpotential could be reduced by introducing water. However, increasing deionized water caused considerably more hydrogen evolution. The dual-electrolyte system using 3 M KOH anhydrous methanol anolyte significantly suppressed parasitic reaction and provided the highest specific capacity of 2328 mAh/g_{Al} at a current density of 10 mA·cm^{-2}. The battery generated Al utilization percentage of 78%. Increasing the water content led to greater discharge voltage and increased the current density but reduced the Al utilization percentage. Thus, the results affirm that the dual-electrolyte system with circulating methanol-based anolyte can significantly suppress corrosion and thereby enhance the capacity of AABs. The dual-electrolyte system is an effective approach and can be applied in other battery systems.

Author Contributions: Conceptualization, S.K.; methodology, P.T. and S.K.; investigation: P.T. and W.K.-i.; formal analysis, P.T. and S.K.; writing—original draft preparation, P.T. and S.K.; writing—review and editing, W.K.-i., M.T.N., T.Y., R.C., and S.K.; supervision, S.K.; funding acquisition, S.K.; project administration, S.K. All authors have read and agreed to the published version of the manuscript.

Conflicts of Interest: The authors declare no conflict of interest.

Abbreviations

AAB   aluminum–air battery
ZAB   zinc–air battery
HER   hydrogen evolution reaction
ORR   oxygen reduction reaction
EIS   electrochemical impedance spectroscopy
SEM   scanning electron microscope
AAFB   aluminum–air flow battery
OCV   open-circuit voltage
PTFE   polytetrafluoroethylene

References

1. Liu, Y.; Sun, Q.; Li, W.; Adair, K.R.; Li, J.; Sun, X. A comprehensive review on recent progress in aluminum–air batteries. *Green Energy Environ.* **2017**, *2*, 246–277. [CrossRef]
2. Mokhtar, M.; Talib, M.Z.M.; Majlan, E.H.; Tasirin, S.M.; Ramli, W.M.F.W.; Daud, W.R.W.; Sahari, J. Recent developments in materials for aluminum–air batteries: A review. *J. Ind. Eng. Chem.* **2015**, *32*, 1–20. [CrossRef]
3. Li, Y.; Lu, J. Metal–Air Batteries: Will They Be the Future Electrochemical Energy Storage Device of Choice? *ACS Energy Lett.* **2017**, *2*, 1370–1377. [CrossRef]
4. Rahman, M.A.; Wang, X.; Wen, C. High Energy Density Metal-Air Batteries: A Review. *J. Electrochem. Soc.* **2013**, *160*, A1759–A1771. [CrossRef]
5. Lao-atiman, W.; Bumroongsil, K.; Arpornwichanop, A.; Bumroongsakulsawat, P.; Olaru, S.; Kheawhom, S. Model-Based Analysis of an Integrated Zinc-Air Flow Battery/Zinc Electrolyzer System. *Front. Energy Res.* **2019**, *7*, 15. [CrossRef]
6. Hopkins, B.J.; Shao-Horn, Y.; Hart, D.P. Suppressing corrosion in primary aluminum–air batteries via oil displacement. *Science* **2018**, *362*, 658. [CrossRef]
7. Rashvand avei, M.; Jafarian, M.; Moghanni Bavil Olyaei, H.; Gobal, F.; Hosseini, S.M.; Mahjani, M.G. Study of the alloying additives and alkaline zincate solution effects on the commercial aluminum as galvanic anode for use in alkaline batteries. *Mater. Chem. Phys.* **2013**, *143*, 133–142. [CrossRef]
8. Abedin, S.Z.E.; Endres, F. Electrochemical Behaviour of Al, Al-In and Al-Ga-In Alloys in Chloride Solutions Containing Zinc Ions. *J. Appl. Electrochem.* **2004**, *34*, 1071–1080. [CrossRef]
9. Wang, D.; Li, H.; Liu, J.; Zhang, D.; Gao, L.; Tong, L. Evaluation of AA5052 alloy anode in alkaline electrolyte with organic rare-earth complex additives for aluminium-air batteries. *J. Power Sources* **2015**, *293*, 484–491. [CrossRef]
10. Mori, R. Addition of Ceramic Barriers to Aluminum–Air Batteries to Suppress By-product Formation on Electrodes. *J. Electrochem. Soc.* **2015**, *162*, A288–A294. [CrossRef]
11. Mori, R. A novel aluminium–Air rechargeable battery with Al2O3 as the buffer to suppress byproduct accumulation directly onto an aluminium anode and air cathode. *RSC Adv.* **2014**, *4*, 30346–30351. [CrossRef]
12. Abdel-Gaber, A.M.; Khamis, E.; Abo-Eldahab, H.; Adeel, S. Novel package for inhibition of aluminium corrosion in alkaline solutions. *Mater. Chem. Phys.* **2010**, *124*, 773–779. [CrossRef]
13. Liu, J.; Wang, D.; Zhang, D.; Gao, L.; Lin, T. Synergistic effects of carboxymethyl cellulose and ZnO as alkaline electrolyte additives for aluminium anodes with a view towards Al-air batteries. *J. Power Sources* **2016**, *335*, 1–11. [CrossRef]
14. Mohamad, A.A. Electrochemical properties of aluminum anodes in gel electrolyte-based aluminum-air batteries. *Corros. Sci.* **2008**, *50*, 3475–3479. [CrossRef]
15. Gelman, D.; Shvartsev, B.; Ein-Eli, Y. Aluminum–air battery based on an ionic liquid electrolyte. *J. Mater. Chem. A* **2014**, *2*, 20237–20242. [CrossRef]

16. Zuo, Y.; Yu, Y.; Zuo, C.; Ning, C.; Liu, H.; Gu, Z.; Cao, Q.; Shen, C. Low-Temperature Performance of Al-air Batteries. *Energies* **2019**, *12*, 612. [CrossRef]

17. Wang, L.; Liu, F.; Wang, W.; Yang, G.; Zheng, D.; Wu, Z.; Leung, M.K.H. A high-capacity dual-electrolyte aluminum/air electrochemical cell. *RSC Adv.* **2014**, *4*, 30857–30863. [CrossRef]

18. Koroleva, E.V.; Thompson, G.E.; Hollrigl, G.; Bloeck, M. Surface morphological changes of aluminium alloys in alkaline solution: Effect of second phase material. *Corros. Sci.* **1999**, *41*, 1475–1495. [CrossRef]

19. Weon, J.-I.; Woo, H.-S. Corrosion mechanism of aluminum alloy by ethylene glycol-based solution. *Mater. Corros.* **2013**, *64*, 50–59. [CrossRef]

20. Wang, D.; Zhang, D.; Lee, K.; Gao, L. Performance of AA5052 alloy anode in alkaline ethylene glycol electrolyte with dicarboxylic acids additives for aluminium-air batteries. *J. Power Sources* **2015**, *297*, 464–471. [CrossRef]

21. Wang, J.-B.; Wang, J.-M.; Shao, H.-B.; Zhang, J.-Q.; Cao, C.-N. The corrosion and electrochemical behaviour of pure aluminium in alkaline methanol solutions. *J. Appl. Electrochem.* **2007**, *37*, 753–758. [CrossRef]

22. Wang, J.B.; Wang, J.M.; Shao, H.B.; Chang, X.T.; Wang, L.; Zhang, J.Q.; Cao, C.N. The corrosion and electrochemical behavior of pure aluminum in additive-containing alkaline methanol–water mixed solutions. *Mater. Corros.* **2009**, *60*, 269–273. [CrossRef]

23. Ryu, J.; Jang, H.; Park, J.; Yoo, Y.; Park, M.; Cho, J. Seed-mediated atomic-scale reconstruction of silver manganate nanoplates for oxygen reduction towards high-energy aluminum-air flow batteries. *Nat. Commun.* **2018**, *9*, 3715. [CrossRef] [PubMed]

24. Hosseini, S.; Han, S.J.; Arponwichanop, A.; Yonezawa, T.; Kheawhom, S. Ethanol as an electrolyte additive for alkaline zinc-air flow batteries. *Sci. Rep.* **2018**, *8*, 11273. [CrossRef]

25. Abbasi, A.; Hosseini, S.; Somwangthanaroj, A.; Mohamad, A.A.; Kheawhom, S. Poly(2,6-Dimethyl-1,4-Phenylene Oxide)-Based Hydroxide Exchange Separator Membranes for Zinc–Air Battery. *Int. J. Mol. Sci.* **2019**, *20*, 3678. [CrossRef]

26. Shinagawa, T.; Garcia-Esparza, A.T.; Takanabe, K. Insight on Tafel slopes from a microkinetic analysis of aqueous electrocatalysis for energy conversion. *Sci. Rep.* **2015**, *5*, 13801. [CrossRef]

27. Abdel-Gawad, S.A.; Osman, W.M.; Fekry, A.M. Characterization and corrosion behavior of anodized Aluminum alloys for military industries applications in artificial seawater. *Surf. Interfaces* **2019**, *14*, 314–323. [CrossRef]

28. Hosseini, S.; Lao-atiman, W.; Han, S.J.; Arpornwichanop, A.; Yonezawa, T.; Kheawhom, S. Discharge Performance of Zinc-Air Flow Batteries Under the Effects of Sodium Dodecyl Sulfate and Pluronic F-127. *Sci. Rep.* **2018**, *8*, 14909. [CrossRef]

29. Abdel-Gaber, A.M.; Khamis, E.; Abo-ElDahab, H.; Adeel, S. Inhibition of aluminium corrosion in alkaline solutions using natural compound. *Mater. Chem. Phys.* **2008**, *109*, 297–305. [CrossRef]

30. Moghadam, Z.; Shabani-Nooshabadi, M.; Behpour, M. Electrochemical performance of aluminium alloy in strong alkaline media by urea and thiourea as inhibitor for aluminium-air batteries. *J. Mol. Liq.* **2017**, *242*, 971–978. [CrossRef]

31. Verma, C.; Singh, P.; Bahadur, I.; Ebenso, E.E.; Quraishi, M.A. Electrochemical, thermodynamic, surface and theoretical investigation of 2-aminobenzene-1,3-dicarbonitriles as green corrosion inhibitor for aluminum in 0.5M NaOH. *J. Mol. Liq.* **2015**, *209*, 767–778. [CrossRef]

32. Mori, R. All solid state rechargeable aluminum–air battery with deep eutectic solvent based electrolyte and suppression of byproducts formation. *RSC Adv.* **2019**, *9*, 22220–22226. [CrossRef]

33. Avoundjian, A.; Galvan, V.; Gomez, F.A. An Inexpensive Paper-Based Aluminum-Air Battery. *Micromachines* **2017**, *8*, 222. [CrossRef] [PubMed]

34. Wang, Y.; Pan, W.; Kwok, H.; Lu, X.; Leung, D.Y.C. Low-cost Al-air batteries with paper-based solid electrolyte. *Energy Procedia* **2019**, *158*, 522–527. [CrossRef]